INTERNATIONAL JOURNAL FOR NUMERICAL METHODS IN FLUIDS
Int. J. Numer. Meth. Fluids 2003; **41**:601–613 (DOI: 10.1002/fld.456)

Linear stability analysis of flow in a periodically grooved channel

T. Adachi[1,*] and H. Uehara[2]

[1] *Department of Mechanical Engineering, Akita University, Tegata-Gakuen, Akita 010-8502, Japan*
[2] *President of Saga University, Saga University, Honjo, Saga 840-8502, Japan*

SUMMARY

We have conducted the linear stability analysis of flow in a channel with periodically grooved parts by using the spectral element method. The channel is composed of parallel plates with rectangular grooves on one side in a streamwise direction. The flow field is assumed to be two-dimensional and fully developed. At a relatively small Reynolds number, the flow is in a steady-state, whereas a self-sustained oscillatory flow occurs at a critical Reynolds number as a result of Hopf bifurcation due to an oscillatory instability mode. In order to evaluate the critical Reynolds number, the linear stability theory is applied to the complex laminar flow in the periodically grooved channel by constituting the generalized eigenvalue problem of matrix form using a penalty-function method. The critical Reynolds number can be determined by the sign of a linear growth rate of the eigenvalues. It is found that the bifurcation occurs due to the oscillatory instability mode which has a period two times as long as the channel period. Copyright © 2003 John Wiley & Sons, Ltd.

KEY WORDS: stability; spectral element method; eigenvalue problem; periodically grooved channel

1. INTRODUCTION

A complex laminar flow in streamwise periodically grooved channels is often encountered in engineering practice, mostly in plate-type compact heat exchangers or cooling systems of micro scale electronic components. Spatially periodic disturbance promoters such as fins or grooves extend heating surface areas, increase fluid mixing and interrupt the development of the thermal boundary layer, leading to enhancement of heat transfer. Therefore, much research has been carried out until now both experimentally and numerically.

Several experiments of flow visualization for the channels with rectangular grooves or rectangular fins showed that at the entrance region two or three grooves are required for the flow to become a fully developed flow state, where the velocity profile repeats itself from groove to groove [1–3]. Namely, the influence of the entrance region can be neglected after two or three grooves, if the channels are sufficiently long and have many grooves. Furthermore, it was shown that the flow is in a two-dimensional steady-state for a relatively small Reynolds number and it becomes a two-dimensional self-sustained oscillatory flow by undergoing a bifurcation at a certain critical Reynolds number.

* Correspondence to: T. Adachi, Department of Mechanical Engineering, Akita University, Tegata-Gakuen, Akita 010-8502, Japan.

Received 1 December 2001
Revised 4 November 2002

In a numerical study, the channels are often divided into identical modules in the streamwise direction assuming that the fully developed velocity field repeats itself in a cyclic manner. This enables us to confine the calculation domain to cover only one of these modules without dealing with the entrance region. Such a procedure was first suggested by Patankar *et al.* [4] and was applied to a configuration consisting of successive ranks of isothermal plate segments placed transverse to the main flow direction under steady-state conditions. In a channel with rectangular grooves on one side of plates, Sunden and Trollheden [5] studied the laminar convective flow and heat transfer under two-dimensional steady-state conditions. Ghadder *et al.* [6] and Pereira and Sousa [7] carried out numerical simulation of the two-dimensional time-dependent Navier–Stokes equation and found that the steady-state flow becomes periodic in time, that is to say, it becomes a self-sustained oscillatory flow at the critical Reynolds number. A wave is generated for the self-sustained flow and this wave is identified as the Tollmien–Schlichting wave. Recently, Adachi and Uehara [8] studied the transitions of flow in five different kinds of channel geometry with rectangular grooves, and obtained the critical Reynolds numbers. Furthermore, Amon [9] presented direct numerical simulation of two- and three-dimensional flows in a periodically grooved channel and showed that the two-dimensional steady flow is stable in regard to any three-dimensional infinitesimal perturbation up to the critical Reynolds number where a two-dimensional, self-sustained oscillatory flow occurs. That is to say, the bifurcation phenomenon is generated in the two-dimensional region.

As mentioned previously, the bifurcation from the steady-state flow to the oscillatory flow has been investigated by numerical simulation. On the other hand, as a representative method to find the critical condition of the bifurcation, there is a method which constitutes an eigenvalue problem based on the linear stability theory. The theory of stability has been applied to simple parallel flows whose velocity distributions depend only upon a space variable and has been devoted to solving the Orr-Sommerfeld equation [10]. Two-dimensional and axis-symmetric flows including a plane Poiseuille flow, Blasius boundary layer, free mixing layers, jet and wake belong to the category of simple flows. However, those flows that have more complex velocity distributions have been left untouched since semi-analytical methods which were useful for the simple flows become difficult for the complex flows and cannot constitute the eigenvalue problem for complex flows applying the linear stability theory. Thanks to recent progress in high-speed computation technology, numerical analysis of the stability problem for simple but non-parallel flows has gradually become available.

In this paper, we investigate the linear stability of the complex laminar flow in a periodically grooved channel. The linear stability theory is applied to the complex flow by using the spectral element method. The generalized eigenvalue problem of matrix form is constituted based on the linear stability theory. We evaluate the critical Reynolds number where the two-dimensional steady flow bifurcates to the two-dimensional self-sustained oscillatory flow, and also clarify the hydrodynamic nature of instability.

2. MATHEMATICAL FORMULATION

2.1. Basic equation

We consider a parallel plate channel which consists of streamwise periodic modules with rectangular expanded grooves on one side as shown in Figure 1(a). Figure 1(b) is an

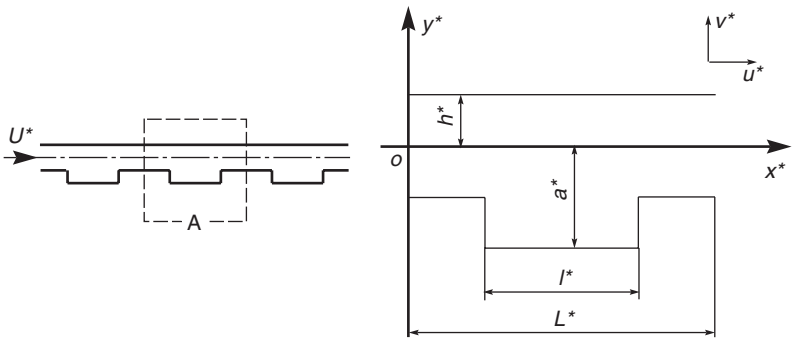

Figure 1. Geometry and co-ordinate: (a) periodically grooved channel; (b) one of the periodic modules.

enlargement of part A shown in Figure 1(a) which is one of the periodic modules and indicates the geometric quantities that define its shape. The x-axis is taken in the flow direction and the y-axis is perpendicular to it with the origin O as shown in Figure 1(b). As non-dimensional parameters to characterize the channel configuration, period L, width l of the groove, and height a of the groove from the centerline between the parallel plates are defined as

$$L = \frac{L^*}{h^*}, \quad l = \frac{l^*}{h^*}, \quad a = \frac{a^*}{h^*} \tag{1}$$

where h^* is the representative length and we represent physical quantities with their dimensions by attaching a superscript * to them. The channel consists of parallel plates without grooves for $a = 1$.

The flow is assumed to be two-dimensional and incompressible. Then, the velocity $\mathbf{u} = (u, v)$ and the pressure p of the flow are governed by the continuity and Navier–Stokes equations as

$$\nabla \cdot \mathbf{u} = \mathbf{0} \tag{2}$$

$$\frac{\partial \mathbf{u}}{\partial t} + (\mathbf{u} \cdot \nabla)\mathbf{u} = -\nabla p + \frac{1}{Re}\nabla^2 \mathbf{u} \tag{3}$$

where length has been made dimensionless with the half height of the channel h^*, velocities with $U^* = 3U_m^*/2$ (U_m^* is the mean velocity at the cross section of height $2h^*$) and time with U^*/h^*. The Reynolds number is defined as $Re = U^* h^*/v^*$, where v^* is the kinematic viscosity.

We assume that the velocity is zero on the plates and adopt the case that the flow rate is fixed in time. Thus, the imposed flow rate $2U_m^* h^*$ is constant and its nondimensional value is $4/3$ in this case. The boundary conditions on the plates are given as

$$\mathbf{u}(\mathbf{x}, \mathbf{t}) = 0 \tag{4}$$

After a short entrance region, the flow is expected to attain a periodic fully developed regime. Thus, the following periodic boundary conditions are imposed as

$$\mathbf{u}(x + mL, y, t) = \mathbf{u}(x, y, t) \tag{5}$$

where m is an integer periodicity index. In this study, we adopt $m=1$ and 2, while m is taken as $m=1$ in many other previous studies [5–9].

For the pressure, we require

$$p = -\beta x + \tilde{p} \tag{6}$$

$$\tilde{p}(x+mL, y, t) = \tilde{p}(x, y, t) \tag{7}$$

where the term $\beta = \beta(t)$ is the driving force for the flow, and is determined by the imposed constant flow-rate condition as

$$\int_{-1}^{1} u(x=0, y, t)\,\mathrm{d}y = \frac{4}{3} \tag{8}$$

In order to simplify the mathematical formulation, we introduce a penalty-function method [11, 12], where the divergence-free condition of Equation (2) is reduced to express a limiting state in which the divergence of the velocity is not zero but extremely small. Then, the pressure $\tilde{p}$ is replaced as

$$\tilde{p} = -\lambda\left(\frac{\partial u}{\partial x} + \frac{\partial v}{\partial y}\right) \tag{9}$$

where λ is a penalty number of order $O(10^8)$. Substituting Equation (9) into Equation (3), we can eliminate $\tilde{p}$ and obtain the basic equations as

$$\frac{\partial u}{\partial t} + u\frac{\partial u}{\partial x} + v\frac{\partial u}{\partial y} = \beta + \lambda\frac{\partial}{\partial x}\left(\frac{\partial u}{\partial x} + \frac{\partial v}{\partial y}\right) + \frac{1}{Re}\left(\frac{\partial^2 u}{\partial x^2} + \frac{\partial^2 u}{\partial y^2}\right) \tag{10}$$

$$\frac{\partial v}{\partial t} + u\frac{\partial v}{\partial x} + v\frac{\partial v}{\partial y} = \lambda\frac{\partial}{\partial y}\left(\frac{\partial u}{\partial x} + \frac{\partial v}{\partial y}\right) + \frac{1}{Re}\left(\frac{\partial^2 v}{\partial x^2} + \frac{\partial^2 v}{\partial y^2}\right) \tag{11}$$

2.2. Steady state equation

The flow is expected to attain its steady-state after enough time at a relatively low Reynolds number. The non-linear steady-state solution $(\bar{U}(x, y), \bar{V}(x, y), \bar{\beta})$ is calculated directly from the steady-state equations which are obtained by dropping the terms including the operator $\partial/\partial t$ in Equations (10) and (11) as

$$\bar{U}\frac{\partial \bar{U}}{\partial x} + \bar{V}\frac{\partial \bar{U}}{\partial y} = \bar{\beta} + \lambda\frac{\partial}{\partial x}\left(\frac{\partial \bar{U}}{\partial x} + \frac{\partial \bar{V}}{\partial y}\right) + \frac{1}{Re}\left(\frac{\partial^2 \bar{U}}{\partial x^2} + \frac{\partial^2 \bar{U}}{\partial y^2}\right) \tag{12}$$

$$\bar{U}\frac{\partial \bar{V}}{\partial x} + \bar{V}\frac{\partial \bar{V}}{\partial y} = \lambda\frac{\partial}{\partial y}\left(\frac{\partial \bar{U}}{\partial x} + \frac{\partial \bar{V}}{\partial y}\right) + \frac{1}{Re}\left(\frac{\partial^2 \bar{V}}{\partial x^2} + \frac{\partial^2 \bar{V}}{\partial y^2}\right) \tag{13}$$

The boundary conditions for $(\bar{U}(x, y), \bar{V}(x, y))$ on the plates are given by

$$\bar{U} = \bar{V} = 0. \tag{14}$$

Those for the periodicity are written as

$$\bar{U}(x+mL, y)=\bar{U}(x, y), \quad \bar{V}(x+mL, y)=\bar{V}(x, y) \tag{15}$$

In addition to these conditions, the constant flow-rate condition is imposed as

$$\int_{-1}^{1} \bar{U}(x=0, y)\,\mathrm{d}y=\frac{4}{3} \tag{16}$$

2.3. Disturbance equation

All the steady-state solutions obtained from Equations (12) and (13) are not stable. We investigate the linear stability of the steady solutions by adding perturbation to them and observing the time dependence for the perturbation. Thus, we consider a perturbation added to the steady solution. Then, the velocity and pressure gradient are expressed as the sum of the steady solution $(\bar{U}(x, y), \bar{V}(x, y), \bar{\beta})$ and the disturbance $(\hat{u}(x, y, t), \hat{v}(x, y, t), \hat{\beta}(t))$ as

$$u=\bar{U}+\hat{u}, \quad v=\bar{V}+\hat{v}, \quad \beta=\bar{\beta}+\hat{\beta} \tag{17}$$

The disturbance is assumed to have the time dependence expressed as

$$\hat{u}=u' \exp(\sigma t), \quad \hat{v}=v' \exp(\sigma t), \quad \hat{\beta}=\beta' \exp(\sigma t) \tag{18}$$

where σ in Equation (18) is a complex number, and the real part $\mathrm{Re}[\sigma]$ and the imaginary part $\mathrm{Im}[\sigma]$ denote the linear growth rate and the frequency of the disturbance, respectively. The steady solution is unstable if $\mathrm{Re}[\sigma]>0$ and the disturbance grows with time. There are two types of instability, as follows. One is that the steady solution is unstable in regard to a stationary disturbance and it bifurcates to another steady solution if $\mathrm{Im}[\sigma]=0$ when $\mathrm{Re}[\sigma]$ vanishes. Such a transition is classified into a pitchfork, saddle-node or transcritical bifurcation by the bifurcation theory. The other is that the steady solution is unstable in regard to an oscillatory disturbance and it bifurcates to a periodic solution with a frequency of $\Omega=\mathrm{Im}[\sigma]/(2\pi)$ if $\mathrm{Im}[\sigma] \neq 0$ when $\mathrm{Re}[\sigma]$ vanishes. Such a transition is called a Hopf bifurcation.

Substituting Equation (18) into Equations (10) and (11), then subtracting the steady-state equations from the resultant equations and dropping the nonlinear terms of the disturbance $(u'(x, y), v'(x, y), \beta')$, we obtain the following linearized equations for the disturbance as

$$\begin{aligned}\sigma u'=&-\bar{U}\frac{\partial u'}{\partial x}-u'\frac{\partial \bar{U}}{\partial x}-\bar{V}\frac{\partial u'}{\partial y}-v'\frac{\partial \bar{U}}{\partial y}+\beta'+\lambda\frac{\partial}{\partial x}\left(\frac{\partial u'}{\partial x}+\frac{\partial v'}{\partial y}\right)\\&+\frac{1}{Re}\left(\frac{\partial^2 u'}{\partial x^2}+\frac{\partial^2 u'}{\partial y^2}\right)\end{aligned} \tag{19}$$

$$\sigma v'=-\bar{U}\frac{\partial v'}{\partial x}-u'\frac{\partial \bar{V}}{\partial x}-\bar{V}\frac{\partial v'}{\partial y}-v'\frac{\partial \bar{V}}{\partial y}+\lambda\frac{\partial}{\partial y}\left(\frac{\partial u'}{\partial x}+\frac{\partial v'}{\partial y}\right)+\frac{1}{Re}\left(\frac{\partial^2 v'}{\partial x^2}+\frac{\partial^2 v'}{\partial y^2}\right) \tag{20}$$

The boundary conditions for $(u'(x, y), v'(x, y))$ are the same as Equations (14) and (15) for $(\bar{U}(x, y), \bar{V}(x, y))$. The flow-rate condition for the disturbance is imposed as

$$\int_{-1}^{1} u'(x=0, y)\,\mathrm{d}y=0 \tag{21}$$

3. NUMERICAL METHOD

The numerical calculations are carried out by utilizing the spectral element method [13–15]. In the spectral element method, the actual solution domain is broken up into K elements and each element is mapped from the physical (x, y) space to the local $(\bar{x}, \bar{y})$ co-ordinate system whose ranges are $[-1, 1]$. The velocity is expanded by high-order Lagrangian interpolants through Gauss–Lobatto–Chebyshev collocation points, defined as

$$\begin{pmatrix} \bar{U}^k(\bar{x}, \bar{y}) \\ \bar{V}^k(\bar{x}, \bar{y}) \\ u'^k(\bar{x}, \bar{y}) \\ v'^k(\bar{x}, \bar{y}) \end{pmatrix} = \sum_{m=0}^{N} \sum_{n=0}^{N} \begin{pmatrix} \bar{U}^k_{mn} \\ \bar{V}^k_{mn} \\ u'^k_{mn} \\ v'^k_{mn} \end{pmatrix} h_m(\bar{x}) h_n(\bar{y}), \quad (k = 1, 2, \ldots, K) \tag{22}$$

where the interpolants are expressed as

$$\begin{aligned} h_i(\bar{\zeta}) &= \frac{2}{N} \sum_{n=0}^{N} \frac{1}{\bar{c}_j \bar{c}_n} T_n(\bar{\zeta}_j) T_n(\bar{\zeta}) \\ \bar{c}_l &= \begin{cases} 1, & l \neq 0, N \\ 2, & l = 0, N \end{cases} \end{aligned} \tag{23}$$

where the T_n are the nth order Chebyshev polynomials and $i = m, n$ and $\bar{\zeta} = \bar{x}, \bar{y}$. The Gauss–Lobatto points are defined as

$$\bar{\zeta}_j = \cos \frac{\pi j}{N}, \quad j = 0, 1, \ldots, N \tag{24}$$

Substituting the expansions of Equation (22) into the weak forms of the steady-state and disturbance equations and also using the Galerkin method, we obtain a set of algebraic equations for the coefficients of the expansions. To construct the system matrix from the element matrices, the direct stiffness method is used [11]. The set of algebraic equations for the steady solution are solved numerically by the Newton–Raphson method. On the other hand, the set of algebraic equations for the stability of the steady solution constitutes a generalized eigenvalue problem in a matrix form as

$$\mathbf{A}\mathbf{a} = \sigma \mathbf{B}\mathbf{a} \tag{25}$$

where $\mathbf{a}$ is a vector of expansion coefficients, and $\mathbf{A}$ and $\mathbf{B}$ are the matrices arising from the right-hand side and left-hand side of Equations (19) and (20), respectively. The eigenvalue σ, with maximum real part, determines the stability characteristics of the steady solution and the corresponding eigenvector represents the flow fields of the disturbance. The eigenvalue problem is solved numerically by a QR method using a standard package contributed from EISPACK. On the other hand, for the cases of large scale eigenvalue problems, a computation of all eigenvalues would be prohibitive. In such cases, Arnoldi's method or simultaneous inverse iteration method are often used to reduce the size of matrix and to find a few eigenvalues [16–18].

4. RESULTS

We have conducted numerical calculations for the geometry of parameters $L = 6.6666$, $l = 2.2222$ and $a = 2.1111$ which corresponds to the same channel that Ghadder *et al.* [6] and Pereira and Sousa [7] investigated.

4.1. Numerical check

First, we check the numerical accuracy. All the calculations are made by double precision. The pressure gradient ratio and eigenvalues for $m = 1$ at $Re = 525$ are calculated for the truncation parameters $N = 14, 16, 18$ and 20, and tabulated in Table I, where the eigenvalues are depicted up to the third unstable mode. The first and the second eigenvalues are real numbers and the third one is a complex number. It is found that $N = 18$ is enough to obtain three to four significant digits. So, the values of the truncation parameter are hereafter taken as $N = 18$. The computational domain and a typical spectral mesh for $N = 18$ are shown in Figure 2 for both $m = 1$ and 2, respectively.

In addition to the convergence, the eigenvalue of the third unstable mode should be compared with the result of Ghadder *et al.* [6]. They obtained the linear growth rate and frequency from numerical simulation of the initial-value problem of the linearized disturbance equation to the Navier–Stokes equations. Our result is in good agreement with that of Ghadder *et al.* [6].

4.2. Steady state solution

The streamlines of the steady-state flow at $Re = 50$, 525 and 1000 are depicted in Figure 3 for both $m = 1$ and 2. The flow is from left to right. The contour levels for the flow field

Table I. Convergence of the pressure gradient and eigenvalues for $m = 1$ at $Re = 525$. σ_1, σ_2 and σ_3 are eigenvalues for the most unstable, second unstable and third unstable modes, respectively.

N	β/β_p	σ_1	σ_2	σ_3
14	0.9724	−0.01852	−0.03780	(−0.03905, 0.1424)
16	0.9726	−0.01853	−0.03782	(−0.03944, 0.1427)
18	0.9726	−0.01853	−0.03783	(−0.04010, 0.1425)
20	0.9725	−0.01854	−0.03784	(−0.03996, 0.1424)
Ghadder *et al.* [6]	—	—	—	(−0.043, 0.142)

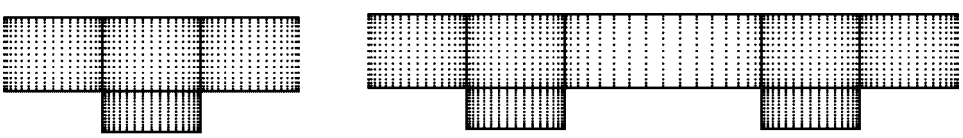

(a) (b)

Figure 2. A plot of the spectral element mesh. The filled circles represent the Chebyshev grid points. The thin solid lines correspond to the spectral element boundaries. (a) Channel for $m = 1$. The amount of the elements is $K = 4$. (b) Channel for $m = 2$. The amount of the elements is $K = 7$.

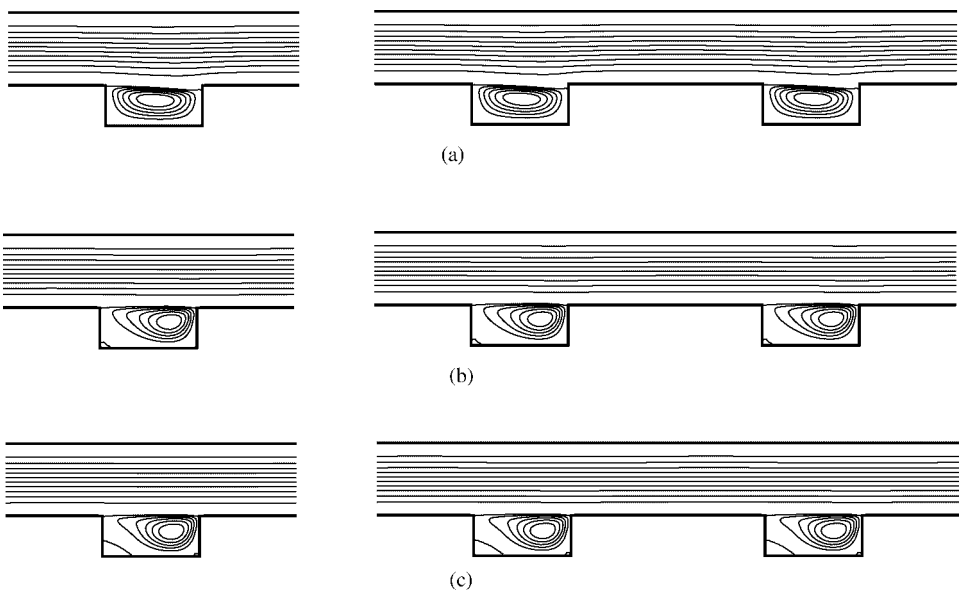

Figure 3. Streamlines of steady-state solution. (a) $Re = 50$, (b) $Re = 525$, (c) $Re = 1000$.

have been chosen to detail the recirculating region. The flow is periodically fully developed and has the same period L as the module, say $m = 1$, independent of the fact of whether m is 1 or 2. A vortical flow motion can be seen in the groove for $Re = 50$ and the main flow deflects into the groove. A shear layer between the main flow and the flow inside the groove is established, which is indicated by the streamline separating from the wall. The center of the vortex moves downstream as the Reynolds number increases. The main flows at $Re = 525$ and 1000 are straight without deflection and become almost parallel, similar to the profile of a plane Poiseuille flow in a parallel plate channel. These results are similar to some previous studies and the qualitative behavior, such as the vortical flow motion and the formation of the shear layer at the groove edge shown here, agrees well with the results of these studies [1–9].

Furthermore, we define the quantity β/β_p to be the ratio of the pressure gradient β to the corresponding quantity for the plane Poiseuille flow (i.e. no groove) $2/Re$, and show it in Figure 4 against the Reynolds number together with the result of Ghadder *et al.* [6]. It is found that the pressure drop ratio is less than unity, showing that the pressure drop is less than the corresponding quantity for the plane Poiseuille flow for the specified flow rate of Equation (8). This is mainly because friction is decreased at the shear layer between the main flow and the flow inside the groove. As shown in a later section, when the Reynolds number undergoes a critical value, the steady-state flow becomes unstable for infinitesimal disturbances and bifurcates to a time-periodic, self-sustained oscillatory flow. The oscillatory flow induces a Reynolds stress responsible for the increase in momentum diffusion, which converts energy from the main flow to the oscillatory flow and sustains it. As the result, the pressure drop of the main flow may increase with the occurrence of the oscillatory flow.

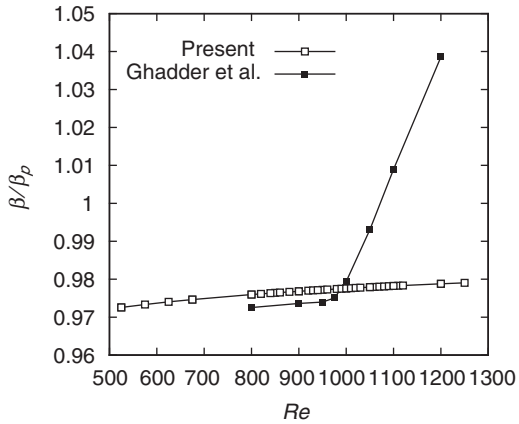

Figure 4. The pressure drop ratio against the Reynolds number.

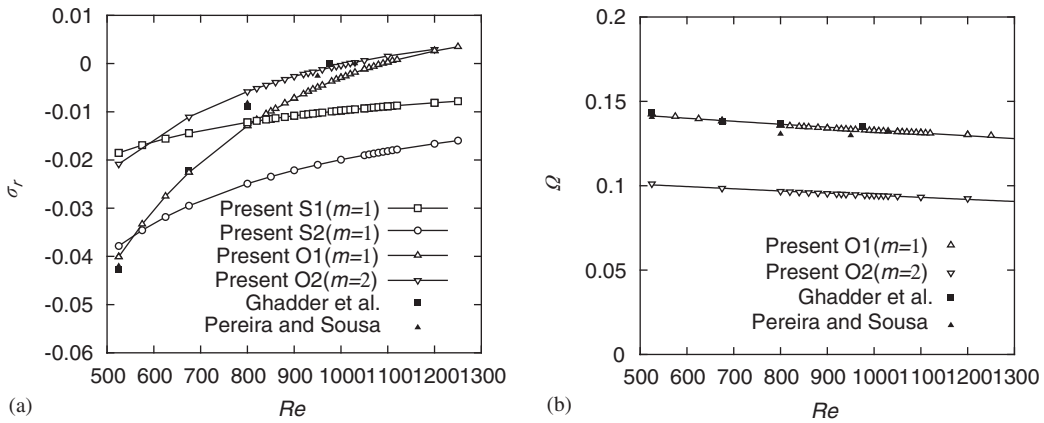

Figure 5. The linear growth rate and frequency. (a) Linear growth rate σ_r. (b) Frequency Ω for the oscillatory disturbance.

Ghadder *et al.* [6] obtained the pressure gradient ratio under unsteady condition and showed that the ratio linearly increases after the bifurcation as shown in Figure 4.

4.3. Linear stability

Now we investigate the linear stability of the steady solutions and plot the dependence of the linear growth rate σ_r and frequency Ω of the oscillatory instability mode on Reynolds number Re in Figure 5, where the linear growth rate is depicted up to the fourth unstable mode. Among the disturbance modes, two are stationary modes which are indicated by S1 and S2, and the other two are oscillatory ones which are indicated by O1 and O2. S1, S2 and O1 are the modes of $m = 1$, while O2 is that of $m = 2$.

Table II. Critical Reynolds numbers and frequencies.

	Re_c	Ω_c
$m=1$		
Present result O1 ($m=1$)	1092	0.1314
Ghadder *et al.* [6]	975	0.141
Pereira and Sousa [7]	1030	0.131
$m=2$		
Present result O2 ($m=2$)	1016	0.09416

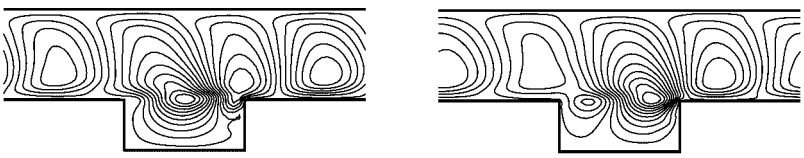

Figure 6. The disturbance streamlines at the criticality $Re_c = 1092$ for O1($m=1$) mode. (a) Real part of the disturbance. (b) Imaginary part of the disturbance.

At $Re = 525$, the most unstable mode is a stationary instability mode, although Ghadder *et al.* [6] and Pereira and Sousa [7] obtained the linear growth rate of the oscillatory mode at the same Reynolds number. They carried out numerical simulation to the time-dependent Navier–Stokes equations using as an initial condition the exact eigenfunction for the most unstable Orr-Sommerfeld mode in the parallel plate channel, and obtained the growth rate and frequencies from the time history of the perturbation velocity at a representative point. Their results coincide with our result for O1 of $m=1$ in the growth rates and frequencies as shown in Figure 5.

As the Reynolds number increases, the linear growth rates for the oscillatory modes increase and become the most unstable and the second unstable modes after $Re \sim 800$, and the sign of the growth rate changes from a negative value to a positive one. Then, the critical Reynolds number is obtained for the oscillatory mode, where the Hopf bifurcation occurs. The critical Reynolds numbers and the corresponding frequencies for the O1 and O2 modes are tabulated in Table II together with the results of Ghadder *et al.* [6] and Pereira and Sousa [7]. The critical Reynolds number for O1 of the present study is slightly larger than the other results, while the corresponding frequency shows good agreement with the result of Pereira and Sousa [7]. However, it should be noted that the critical Reynolds number $Re_c = 1016$ for $m=2$ is smaller than $Re_c = 1092$ for $m=1$. Thus we can conclude that the critical mode is given by $m=2$, and the critical Reynolds number is $Re_c = 1016$.

To determine the nature of the hydrodynamic instability, we plot the disturbance streamlines for the O1 and O2 modes at criticality Re_c in Figures 6 and 7, which correspond to the real and imaginary parts of the eigenvector of each mode. In the disturbance streamlines, there are two pairs of vortices which span L in the disturbance field of the $m=1$ mode as shown in Figure 6, while there are three pairs of vortices which span $2L$ of the channel in the disturbance field of $m=2$ as shown in Figure 7. It is evident that the vortices which become

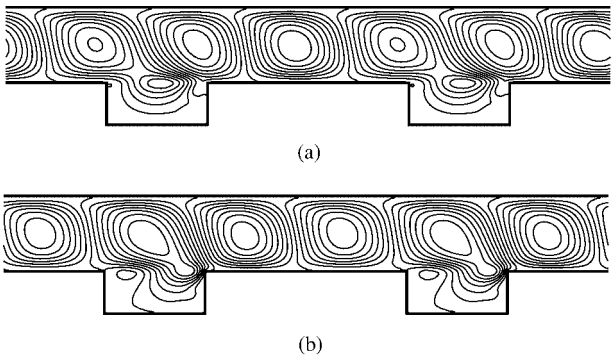

Figure 7. The disturbance streamlines at the criticality $Re_c = 1016$ for O2($m = 2$) mode. (a) Real part of the disturbance. (b) Imaginary part of the disturbance.

a pair of the odd number cannot appear in the channel as $m = 1$. However, as we have seen, the mode of $m = 2$ gives the critical Reynolds number. This indicates that the calculation should be carried out as $m = 2$ in such a channel with the periodic grooves, although such a phenomenon is greatly dependent on the channel geometry.

As mentioned in Ghadder *et al.*, the instability mode for the grooved channel very closely resembles a traveling Tollmien–Schlichting wave particularly in the flow structure and the dispersive relation between the frequency and the wave number $\alpha = 2\pi n/L$, where n is the number of waves that spans the periodicity length L. In the present study, the frequencies of O1 and O2 at the criticality are 0.1314 and 0.09416 as shown in Table II. On the other hand, those of the Tollmien–Schlichting wave in the parallel plate channel which correspond to the critical Reynolds numbers of O1 and O2 are 0.1346 and 0.09090, respectively. Therefore, we can consider that the disturbance mode of O2 is the Tollmien–Schlichting mode as well as that of O1, although they are somewhat modified due to the need for adaptation to a more complex geometry than that of the parallel-plate channel. Similar self-sustained oscillatory flows at Tollmien–Schlichting frequencies were found in other modified channel geometries such as in channels with cylindrical promoters [19] and communicating channels [20].

It is found that the Hopf bifurcation occurs at a small Reynolds number for a periodically grooved channel compared with the fact that the plane Poiseuille flow is destabilized by the Tollmien–Schlichting wave for $Re > 5772$ [21]. This is mainly because the Kelvin–Helmholtz instability, which is established at the groove lip due to the formation of inflections in the passage velocity profile, forces the normally damped Tollmien–Schlichting wave of the outer grooves and projects energy onto it. As a result of complex interaction, it results in two-dimensional traveling waves at moderately low Reynolds numbers.

5. CONCLUSIONS

A stability analysis based on the linear theory has been performed for the flow in a channel with periodically grooved parts. From the steady-state and disturbance equations, the generalized eigenvalue problem has been constituted by successfully applying the linear stability theory to the complex flow.

The critical Reynolds numbers and frequencies for the onset of self-sustained oscillations have been obtained for both $m=1$ and 2. It is found that the critical Reynolds number is obtained for the oscillatory mode of $m=2$ instead of $m=1$. This is a main conclusion different from the previous results, because the previous stability analyses by numerical simulation considered only $m=1$. The result obtained here implies that the period of the self-sustained oscillatory flow after the bifurcation becomes the double in the channel period. It is expected that a significant effect might be generated in characteristics of heat transfer, pressure loss and other hydrodynamic properties after the bifurcation depending on whether m is 1 or 2. This can be clarified by the numerical simulation of the time-dependent Navier–Stokes equations.

Finally, the unstable modes of flow in grooved channels are greatly dependent on their shape. It cannot be expected which mode gives the critical mode in advance. Therefore, it is necessary for another calculation about each $m \geqslant 3$, which has not been considered in this study. This is a future problem.

NOMENCLATURE

a	height of groove from the centerline
h^*	half-height of the parallel plane channel
L	period of the module
l	length of groove
p	pressure
Re	Reynolds number, $Re = U^* h^*/\nu^*$
U_m^*	mean velocity at the cross section of height $2h^*$
U^*	representative velocity, $U^* = 3U_m^*/2$
u, v	velocity components in $x-$ and $y-$ directions, respectively
$\mathbf{u}$	velocity vector

Greek symbols

β	pressure gradient
λ	penalty number
ν^*	kinematic viscosity
ρ^*	density
Ω	frequency
σ	eigenvalue $\sigma = \sigma_r + 2\pi\Omega i$

Subscripts

c	critical
p	plane Poiseuille flow

Superscript

$*$	dimensional value

ACKNOWLEDGEMENTS

The authors would like to express their thanks to Professor Y. Ikegami, Institute of Ocean Energy, Saga University (IOES), for his support, and to Miss. A. Ide, secretary at Saga University, for her encouragement. We also would like to thank Miss. S. Hill for helpful comments.

REFERENCES

1. Greiner M. An experimental investigation of resonant heat transfer enhancement in grooved channels. *International Journal of Heat and Mass Transfer* 1991; **34**:1383–1391.
2. Roberts EPL. A numerical and experimental study of transition processes in an obstructed channel flow. *Journal of Fluid Mechanics* 1994; **260**:185–209.
3. Nishimura T, Kunitsugu K, Nakagiri H. Fluid mixing and local mass transfer characteristics in a grooved channel for self-sustained oscillatory flow. *Heat Transfer-Japanese Research* 1998; **27**:522–534.
4. Patankar SV, Liu CH, Sparrow EM. Fully developed flow and heat transfer in ducts having streamwise-periodic variations of cross-sectional area. *ASME Journal of Heat Transfer* 1077; **99**:180–186.
5. Sunden B, Trollheden S. Periodic laminar flow and heat transfer in a corrugated two-dimensional channel. *International Communication of Heat and Mass Transfer* 1989; **16**:215–225.
6. Ghaddar NK, Korczak KZ, Mikic BB, Patera AY. Numerical investigation of incompressible flow in grooved channels. Part1. stability and self-sustained oscillations. *Journal of Fluid Mechanics* 1986; **163**:99–127.
7. Pereira JCF, Sousa JMM. Finite volume calculations of self-sustained oscillations in a grooved channel. *Journal of Computational Physics* 1993; **106**:19–29.
8. Adachi T, Uehara H. Transitions and pressure drop characteristics of flow in channels with periodically grooved parts. *JSME International Journal Series B* 2001; **44**:221–230.
9. Amon AH. Spectral element-Fourier method for transitional flows in complex geometries. *AIAA Journal* 1993;**31**:42–48.
10. Drazin PG, Reid WH. *Hydrodynamic Stability*. Cambridge University Press: Cambridge, 1981 (Chapter 5).
11. Baker AJ. *Finite Element Computational Fluid Mechanics.* McGraw-Hill: New York, 1985 chapter (2).
12. Reddy JN. On penalty function methods in the finite-element analysis of flow problems. *International Journal for Numerical Methods in Fluids* 1982; **2**:151–171.
13. Patera AT. A spectral element method for fluid dynamics: laminar flow in a channel expansion. *Journal of Computational Physics* 1984; **54**:468–488.
14. Karnidakis GE. *Spectrallhp Element Methods for CFD* (Section 2). Oxford University Press: Oxford, 1999.
15. Amon CH. Spectral element methods for unsteady fluid and heat transfer in complex geometries: methodology and applications. *Advances in Numerical Heat Transfer*, vol. 2. Taylor & Francis: London, 2000; 71–108.
16. Eriksson LE, Rizzi A. Computer-aided analysis of the convergence to steady state of discrete approximations to the Euler equations. *Journal of Computational Physics* 1985; **57**:90–128.
17. Fortin A, Jardak M, Gervais JJ, Pierre R. Old and new results on the two-dimensional Poiseuille flow. *Journal of Computational Physics* 1994; **115**:455–469.
18. Stewart WJ, Jennings A. A simultaneous iteration algorithm for real matrices. *ACM Transactions on Mathematical Software* 1981; **7**:184–198.
19. Karnidakis GE, Mikic BB, Patera AT. Minimum dissipation transport enhancement by flow destabilization: Reynolds' analogy revisited. *Journal of Fluid Mechanics* 1988; **192**:365–391.
20. Amon CH, Mikic BB. Spectral element simulations of unsteady forced convective heat transfer. *Numerical Heat Transfer Part A* 1991; **19**:1–19.
21. Orzsag SA. Accurate solution of the orr-sommerfeld stability equation. *Journal of Fluid Mechanics* 1971; **50**:689–703.

